# Self-Diffusion in a Weakly Entangled Associative Network

Irina Mahmad Rasid,† Ameya Rao,‡ Niels Holten-Andersen\*,† and Bradley D. Olsen\*,‡

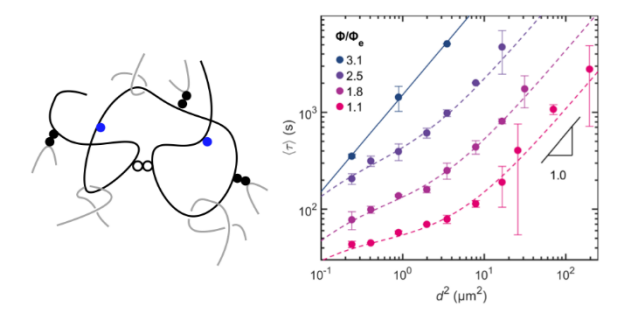
<sup>†</sup> Department of Materials Science and Engineering, Massachusetts Institute of Technology, 77

Massachusetts Avenue, Cambridge, Massachusetts 02139, United States

<sup>‡</sup> Department of Chemical Engineering, Massachusetts Institute of Technology, 77

Massachusetts Avenue, Cambridge, Massachusetts 02139, United States

# For Table of Contents use only



Abstract: The presence of entanglements in associative polymer gels has been shown to impart enhanced mechanical strength, toughness, and extensibility; however, the interplay between topological and binding interactions in these systems remains poorly understood. Here, the effect of entanglements on chain dynamics in a model associative network is investigated in the weakly entangled regime, corresponding to  $1.1-3.1~\phi_e$  where  $\phi_e$  is the characteristic concentration for the onset of entanglement. The associative network is formed by a linear random copolymer of N,N-dimethylacrylamide and a histidine-functionalized monomer cross-linked with Ni<sup>2+</sup> ions. Rheological characterization indicates that the concentrations investigated span the transition from unentangled to the weakly entangled regime, resulting in a subtle broadening of their relaxation spectrum. Self-diffusion measurements using forced Rayleigh scattering demonstrate a pronounced suppression of apparent superdiffusive behavior with increasing concentration, revealing a stronger impact of topological entanglement on self-diffusion compared overall network relaxation. This suppression in superdiffusive behavior is attributed to a reduction in the contribution of "hopping" diffusion due to the presence of entanglements, resulting in an approach to purely Fickian diffusion governed by a single "walking" diffusive mode at the highest concentration probed. These results demonstrate the marked effects of entanglements on selfdiffusion and relaxation in associative networks, providing insight into network response beyond that accessible by rheology alone.

# Introduction

Associative polymer networks are a class of soft materials that has gained interest across many communities due to their tunable viscoelastic behavior, ability to respond to external stimuli, and self-healing abilities.<sup>1-10</sup> While associative networks have shown great versatility, they are often plagued by issues such as erosion and low toughness that limit their use for certain

applications.<sup>11-14</sup> The introduction of topological entanglements into these systems is a potential solution to overcome these issues by providing additional barriers to chain motion.<sup>1, 15, 16</sup> However, understanding the dynamics of entangled associative networks remains an open area of research due the complexity of their viscoelastic and transport properties.<sup>17-21</sup>

Associative network dynamics are largely dictated by the processes of bond association and dissociation, which has served as a basis for the development of several transient network models to date. For networks prepared in the presence of a solvent, i.e., physical gels, the polymer volume fraction  $\phi$  further dictates their properties, resulting in several scaling regimes as developed in the sticky Rouse<sup>23, 26</sup> and sticky reptation<sup>23, 24</sup> models. Two main regimes can be identified based on the entanglement concentration,  $\phi_e$ . In a good solvent,  $\phi_e$  is defined as

$$\phi_e = \left(\frac{N_{e,0}}{N}\right)^{0.8} \tag{1}$$

where  $N_{\rm e,0}$  is the number of monomers between entanglements in a melt and N is the number of monomers in the chain. <sup>23</sup> Below the entanglement limit ( $\phi < \phi_e$ ), chain segments undergo Rouse-like motion that is delayed by the presence of the stickers as detailed in the sticky Rouse model. <sup>23, 26</sup> In the presence of entanglements, the sticky reptation model <sup>24</sup> considers the motion of the chain to be further topologically restricted since it can only diffuse along the contour of the confining tube defined by the entanglements. The sticky reptation model predicts that entangled associative networks show two main relaxation processes, one corresponding to the lifetime of the stickers and a second, low-frequency relaxation regime arising from hindered reptation. In particular, the terminal relaxation should be significantly delayed compared to gels in the unentangled regime. <sup>23, 24</sup> More recent advances in the sticky reptation model have included the effects of constraint release and contour length fluctuations, which can broaden the time scale over

which the relaxation process occurs. <sup>18, 24, 27, 28</sup> Although recent investigations have attempted to experimentally verify the predictions of these sticky reptation models with shear rheology, there has been little study of the *self-diffusion* of the network-forming chains in entangled systems, which would provide an additional test of the dynamic mechanisms invoked in these theories. Self-diffusion in entangled gels is expected to differ significantly from that in unentangled gels due to the cooperative effects of sticker association and topological entanglements in slowing chain motion. In addition, experiments have shown that the linear viscoelastic response of gels in the weakly entangled regime can be very similar to that of unentangled gels, making the transition between unentangled and entangled regimes difficult to identify by rheology alone. <sup>18, 28</sup>

Self-diffusion measurements by forced Rayleigh scattering (FRS) can reveal important insight into the mechanisms of chain motion as a critical test of the associative network theories developed to date.  $^{29-31}$  The experimentally accessible length scales for FRS correspond to 0.5-50  $\mu m^{29-31}$  such that it probes the time scales required for the polymers to diffuse over several times their radius of gyration,  $R_g$ . Self-diffusion measurements of several distinct unentangled associative networks showed phenomenological superdiffusive scaling on length scales corresponding to  $100-1000R_g$ , which transitioned to Fickian scaling on longer length scales.  $^{29-31}$  This behavior was explained by a phenomenological two-state model and showed that superdiffusive scaling in FRS measurements can be due to the presence of two apparent diffusing species with distinct diffusivities.  $^{29}$  From single-chain simulations of associative 4-arm star polymers  $^{32}$  and linear polymers with varying numbers of stickers along the backbone,  $^{33}$  the two diffusive modes were assigned as "walking" and "hopping." Hopping refers to a process in which a molecule releases all of its stickers to undergo relatively unhindered diffusion with a mean-square displacement of several times  $R_g^2$  before reattaching to the network. In contrast, walking

refers to a step-wise diffusive motion where at least one of the stickers remains attached to the network while part of the chain attaches to a new position. Thus, FRS not only provides a method to measure the diffusivity within the networks, but it can also indicate the presence of multiple distinct diffusive modes, providing a detailed description of chain dynamics in these networks beyond that revealed by rheology alone. While the studies performed so far have been on unentangled associative networks, it highlights the potential of FRS as a technique to detect important changes in network dynamics as it undergoes transitions such as the onset of entanglements.

In this study, chain relaxation and self-diffusion in a model associative network above the entanglement threshold were investigated through a combination of shear rheology and FRS. The model system was an associative hydrogel prepared with a low-dispersity linear copolymer of N,N-dimethylacrylamide and a histidine-functionalized monomer such that transient metal-coordinate crosslinks formed upon addition of  $Ni^{2+}$  ions (Figure 1). The concentrations investigated by self-diffusion correspond to the weakly entangled regime, ranging from  $1.1 - 3.1 \, \phi_e$  as calculated using Eq. 1 and  $N_{e,0}$  estimated from Ref<sup>34</sup>. Rheological characterization of gels in this concentration range reveals a broadening of the relaxation spectrum due to the onset of entanglements, while self-diffusion measurements demonstrate a marked suppression of apparent superdiffusive scaling with increasing extent of entanglement. The results highlight the strong role of topological entanglement as an orthogonal hindrance to sticker association, with implications for the design of viscoelastic soft materials with unique transport properties.

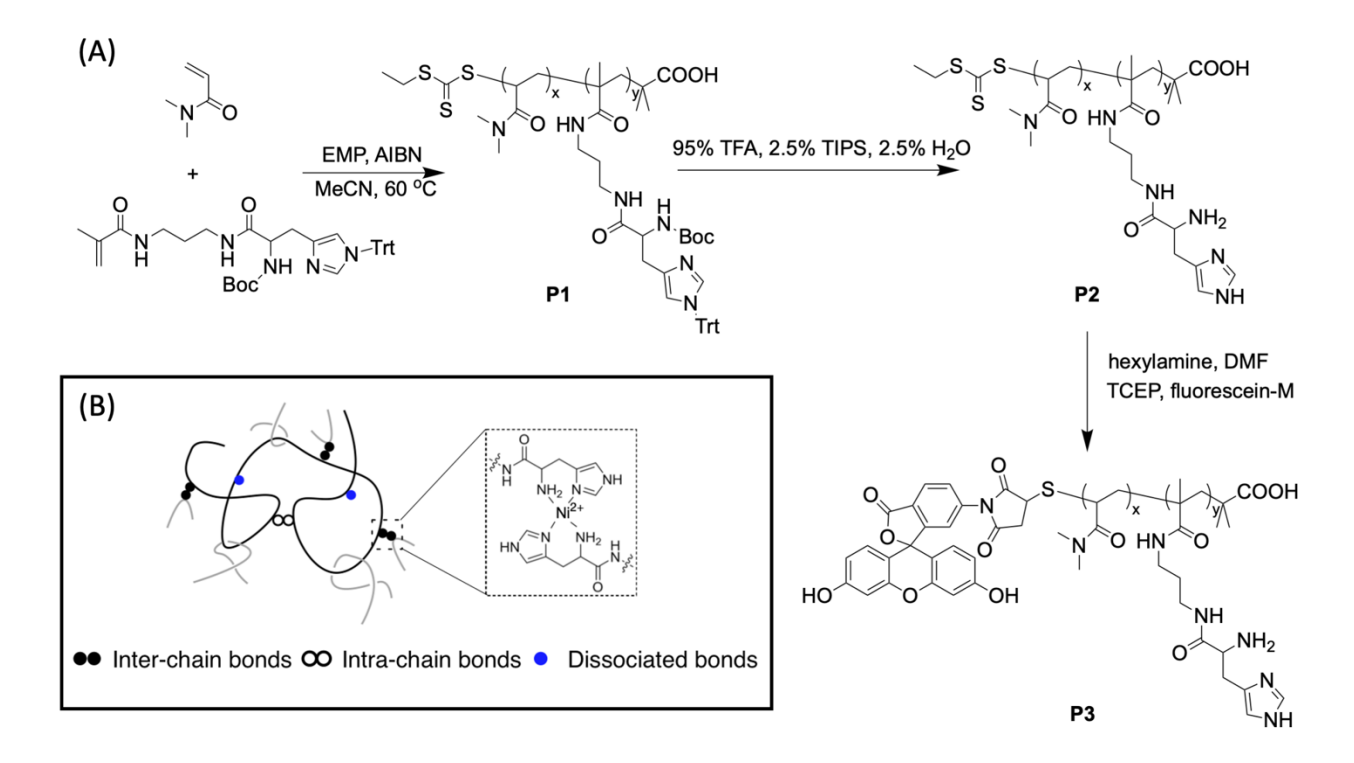


**Figure 1.** (A) Synthesis of linear PDMA polymers with pendant histidine side groups. (B) Schematic of the model associative network prepared with a linear copolymer of N,N-dimethylacrylamide and a histidine-functionalized monomer such that metal-coordinate crosslinks are formed upon addition of  $Ni^{2+}$  ions.

# **Experimental Methods**

**Materials.** N-Boc-Nim-trityl-N-3-methacrylamidopropyl-L-Histidinamide (HisMA) <sup>35</sup> and 2-(ethylthio-carbonothioylthio)-2-methylpropionic acid (EMP) <sup>36</sup> were synthesized following published procedures. Fluorescein-5-maleimide was purchased from ThermoFisher Scientific. *N,N*-Dimethyl-acrylamide (DMA) was purified through a basic alumina column to remove inhibitor before polymerization. All other chemical reagents were purchased from Sigma-Aldrich or VWR and used as received.

Characterization. Gel permeation chromatography (GPC) measurements were performed on an Agilent 1260 LC system with two ResiPore columns in series (300 × 7.5 mm, Agilent Technologies, Santa Clara, CA). The flow rate was set to 1 mL/min at 70 °C, and DMF with 0.02 M LiBr was used as the mobile phase. The molecular weights were determined using a Wyatt miniDAWN TREOS multiangle light scattering detector and a Wyatt Optilab T-rEX differential refractive index detector. NMR spectra were recorded on a Varian 400 MHz spectrometer and the residual undeuterated solvent peaks were used as references (7.27 ppm for CDCl<sub>3</sub> and 4.79 ppm for D<sub>2</sub>O).

Synthesis of high molecular weight PDMA Polymers with Pendant Histidine Side Groups (P2). Homopolymers of DMA and copolymers of DMA and HisMA were synthesized by reversible addition-fragmentation chain transfer (RAFT) polymerization (Figure 1a), using a procedure adapted from ref. 31 to target molar mass of 100 kg mol-1. The total monomer concentration used for polymerization was 2.0 M, with a ratio of 1:0.33 of EMP: azobisisobutyronitrile (AIBN). The ratio of monomers: EMP was kept constant at 1111:1, while the amount of HisMA added was varied between 0 - 1.5 mol% to achieve targeted sticker densities. The MeCN solutions for polymerization were degassed by purging with N<sub>2</sub>, and the polymerizations were then performed at 60 °C until the desired conversion of around 80% was achieved as determined by DMF GPC (approximate polymerization time of around 7 h). The reaction was terminated by opening the reaction flask to air and allowing it to cool to room temperature. The protected polymer P1 was then purified by precipitation into diethyl ether and then dried under vacuum overnight. The molar mass of P1 was determined using DMF GPC prior to the deprotection step (Figure S1, Table S1). The mole fraction of HisMA was determined by <sup>1</sup>H NMR (Figure S2).

The Boc and Trt protecting groups were removed by dissolving the P1 polymers in DCM. Water, triisopropylsilane (TIPS), and trifluoroacetic acid (TFA) were added sequentially to the solution. The mixture was stirred for 2 h at room temperature, after which the volatiles were removed under vacuum. The polymers were then dissolved in MeOH and precipitated into diethyl ether twice. The polymers were then dried under vacuum overnight. Once dried, the polymers were dissolved in 30 mL water, transferred to a centrifugal filter (3kDa MWCO), and spun at 4000 g for 30 minutes. An additional 30 mL of water was added, and the filtration was repeated four times. The polymers were then filtered through a 0.45 µm hydrophilic PVDF syringe filter and lyophilized, yielding polymer P2. The complete removal of the Boc and Trt protecting groups was confirmed by <sup>1</sup>H NMR (Figure S3). The mass and volumes of reactants used and yield for each polymer is shown in the supporting information (Table S2 and Table S3). The polymers have been labeled PDMA-100k (homopolymer) or PDHMS-100k, where S denotes the average number of stickers per chain, while the 100k indicates the molar mass of the polymer.

Synthesis of Fluorescein-Labeled PDMA Polymers (P3). For PDHM7-100k, fluorescein-labelled polymers were synthesized for self-diffusion studies. The deprotected polymers P2 (50 mg, 0.5 μmol) were first dissolved in 2.7 mL DMF, to which hexylamine (1.4 μL, 10 μmol) was added. The reaction was left stirring overnight under nitrogen to ensure complete aminolysis while minimizing undesirable thiol oxidation. Tris(2-carboxyethyl)phosphine hydrochloride (TCEP·HCl, 1.5 mg, 5 μmol) and maleimide-functionalized fluorescein (2.25 mg in 50 μL of DMSO, 5 μmol) were then added to the reaction mixture. The reaction was then left to stir overnight. The solution was then diluted with 30 mL 5% DMSO in water and transferred to a centrifugal filter (3 kDa MWCO), which was spun for 4000 g for 1 h at 4 °C. A further 30 mL of 5% DMSO in water was added, and the process was repeated several times until the spin-through

appeared colorless. A final spin was performed with water to remove the DMSO. The polymers were filtered using a 0.45 µm hydrophilic PVDF syringe filter and finally lyophilized. The product **P3** was obtained as a light yellow powder.

Gel Preparation. The gel preparation procedures for the PDHM polymers were adapted from previous publications. 31, 35 The polymers were first dissolved in a Bis-Tris buffer (100mM, pH 7.0), at a volume adjusted according to the target concentration of the gel. Once the polymers are fully dissolved, the appropriate amount of a stock solution containing 200 mM NiCl<sub>2</sub> and 100 mM Bis-Tris was added so that the ratio of HisMA/Ni was 2:1. The mixture was thoroughly mixed using a 21-gauge needle. Finally, the appropriate amount of a stock solution of 1 M NaOH with 100 mM Bis-Tris was added such that the ratio of HisMa/NaOH was 1:1. The gels were mixed vigorously with a micro spatula and then centrifuged at 21,100 g. The mixing process was repeated several times until a macroscopically homogenous gel was obtained. The gel was then centrifuged a final time to remove air bubbles introduced during the mixing process. The amount of NiCl<sub>2</sub> and NaOH stock solution needed was determined by <sup>1</sup>H NMR (Figure S2).

**Rheology.** Frequency sweep and strain sweep experiments were performed on an Anton Paar 301 Physica rheometer with a stainless-steel cone and plate geometry. The size of the plates used was either 10 mm diameter ( $2^{\circ}$  angle) for gels with a shear modulus above 10 kPa or 25 mm diameter ( $1^{\circ}$  angle) for gels with a shear modulus below 10 kPa. All gel samples were centrifuged at 21,100 g at room temperature until all air bubbles were removed. Once the samples were loaded onto the rheometer, mineral oil was added to the sample edge to minimize dehydration. Experiments were performed over 5-55 °C, with the temperature controlled using a Peltier plate. All frequency sweeps were performed at 1% strain, which was determined to be within the linear viscoelastic region from strain sweep experiments (Figure S4).

Frequency sweeps were fit to the sticky double reptation model<sup>28</sup> and a single-mode Maxwell model. Fitting to the sticky double reptation model was performed separately for each frequency sweep using the RepTate software package,<sup>37</sup> with adjustable parameters  $n_s$  (the number of effective stickers per chain),  $n_e$  (the number of effective entanglements per chain),  $n_s$  (the effective sticker lifetime),  $n_s$  (the entanglement plateau modulus), and  $n_s$  (a dimensionless parameter of order ~1).

Forced Rayleigh Scattering. Self-diffusion measurements were performed by adding 20  $\mu$ M of the fluorescein-labelled polymers (P3) to the dissolved polymer P2 before the NiCl<sub>2</sub> stock solution was added. To remove any dust particles, the buffer solutions for preparing FRS samples were filtered through a 0.2  $\mu$ m PTFE syringe filter prior to mixing solutions. The samples were sealed between two quartz disks (17 mm in diameter) with a Teflon spacer (0.2 mm thick) and annealed at 80 °C for three hours to eliminate shear history from loading. Samples were then equilibrated at the experimental temperature for 1 h before experiments were performed. The procedure for performing FRS measurements has been previously described<sup>29, 38, 39</sup> and will be briefly reviewed here. A continuous wave laser (100 mW,  $\lambda$  = 488 nm) was split into two beams and then refocused onto the sample at an angle  $\theta$ . The constructive interference bleaches the photochromic fluorescein dye and generates an amplitude grating of dye concentration with a characteristic spacing d defined as

$$d = \frac{\lambda}{2\sin(\theta/2)} \tag{2}$$

The exposure time of the sample was in the range of 100-750 ms. Diffusion of the dye-labelled polymers results in a sinusoidal concentration profile that was monitored by diffraction of a single reading beam at the same wavelength. The beam intensity was attenuated by  $10^{-4}$  so that further

bleaching of the dye will not occur and the change in the profile was only due to diffusion. The time constant,  $\tau$ , is then extracted from fitting a sum of two exponential functions to the signal:

$$I = \left(A_1 \exp\left[-\left(\frac{t}{\tau_1}\right)^{\beta_1}\right] + A_2 \exp\left[-\left(\frac{t}{\tau_2}\right)^{\beta_2}\right]\right)^2 + B \tag{3}$$

where I is the intensity,  $\beta$  is the stretched exponent ranging from 0 to 1, and B is the incoherent background and  $\tau_2 > \tau_1$ . Finally, the average decay time constant was calculated as the first moment of the stretched exponential, based on  $\tau_2$ :

$$\langle \tau \rangle = \frac{\tau_2}{\beta_2} \Gamma\left(\frac{1}{\beta_2}\right) \tag{4}$$

where  $\Gamma$  is the gamma function. Representative FRS decays and their fits to Eq. 3 are provided in the Supporting Information.

# Results and Discussion

To study the combined effects of topological entanglement and sticker association on chain dynamics, a model associative network was synthesized comprising an N,N-dimethylacrylamide (DMA) backbone containing pendant histidine moieties, as shown in Fig. 1. Upon the addition of Ni<sup>2+</sup> ions in a 1:2 ratio of Ni<sup>2+</sup>:histidine, transient metal-ligand crosslinks were formed, resulting in a space-spanning gel network. To create topological entanglements in the network, the target molar mass of the network-forming chains was set to 100 kg/mol, and the concentration was varied between  $0.6 - 4.8 \varphi_e$ , where  $\varphi_e \approx 0.12$  is the entanglement volume fraction at this chain length.<sup>34</sup> This allowed study of the transition from the unentangled to the weakly entangled regime in

associative networks as a comparison to prior investigations of unentangled gels of identical backbone and sticker chemistry but smaller chain length.

Evidence of transition to the weakly entangled regime in the viscoelastic properties. The linear viscoelastic properties of the PDHM7-100k gels, as measured with frequency sweeps (Figure 2), demonstrate relaxation behavior qualitatively consistent with the weakly entangled regime. As the concentration is increased from  $0.6-4.8~\phi_e$ , a single high-frequency plateau,  $G_P$ , is seen in the storage modulus, G', ranging from  $0.03-20~\mathrm{kPa}$ , while the crossover frequency,  $\omega_e$  shifts to lower frequencies. Following the crossover of G' and G'' at  $\omega_e$ , terminal relaxation is seen for all concentrations consistent with the classical Maxwell scalings of  $G' \sim \omega^2$  and  $G'' \sim \omega^1$ . Note that additional concentrations (unfilled symbols in Figure 2) were included for the viscoelastic characterization beyond those studied by self-diffusion measurements (filled symbols in Figure 2) to provide further information about the concentration regimes relevant to their

dynamics.

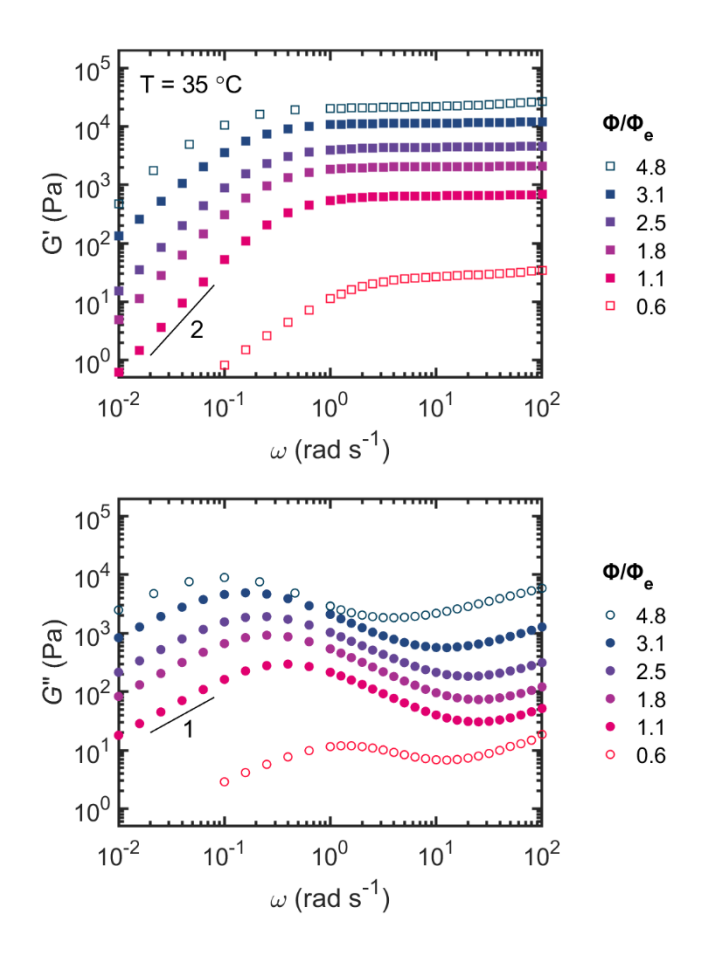


**Figure 2.** Plot of G' and G'' vs  $\omega$  for PDHM7-100k gels (~7 stickers per chain) for concentrations ranging from 0.6-4.8  $\phi/\phi_e$ . All data are collected at 35 °C. Filled symbols correspond to concentrations also investigated by self-diffusion measurements; unfilled symbols were omitted from self-diffusion measurements since the time scales were not experimentally accessible.

The sticky reptation model predicts that for  $\phi > \phi_e$  in a good solvent, the zero-shear viscosity  $\eta_0$  should scale with volume fraction as  $\eta_0 \sim \phi^{3.77}$ , where the strong scaling with concentration for  $\phi > \phi_e$  arises from the increased number of entanglements per chain as the concentration is increased further past  $\phi_e$ .<sup>23</sup> As seen in Figure 3, the PDHM7-100k gels exhibit a scaling of  $\eta_0 \sim \phi^{3.5 \pm 0.8}$  for 1.3 - 4.8  $\phi_e$  above the entanglement threshold, which is close to, but slightly weaker than, the predicted scaling from the sticky reptation model. It should be noted that

the sticky Rouse model<sup>23, 26</sup> predicts for unentangled systems (i.e.,  $\phi < \phi_e$ ) a significantly weaker dependence of  $\eta \sim \phi^{1.17}$ . The intermediate scaling observed in the gels here may arise from a transition between the two regimes due to the onset of entanglement. Previous studies of non-associative entangled linear polymers have shown a transition from the unentangled to the weakly entangled regime at ~2 entanglements per chain, followed by a transition to the strongly entangled regime at ~10 entanglements per chain.<sup>40,41</sup> For associative networks, however, the transition point from unentangled to the entangled regime is harder to define due to the interdependence between segmental chain dynamics and sticker dynamics.<sup>17-19, 24, 28</sup> This may yield an additional plateau in G to account for separate relaxation timescales from sticker or chain dynamics<sup>24, 28</sup> and regions showing different scaling of  $G \sim \omega$  and  $G \sim \omega$  from effects such as constraint release<sup>18, 28</sup> and contour length fluctuations.<sup>18</sup> Although the frequency sweeps of the PDHM7-100k gels do not clearly exhibit these additional features, attempts to fit each frequency sweep with a single Maxwell mode show increasing deviation with concentration, which indicates a broadening of the relaxation timescale most obvious at the highest concentration (Figure S7).

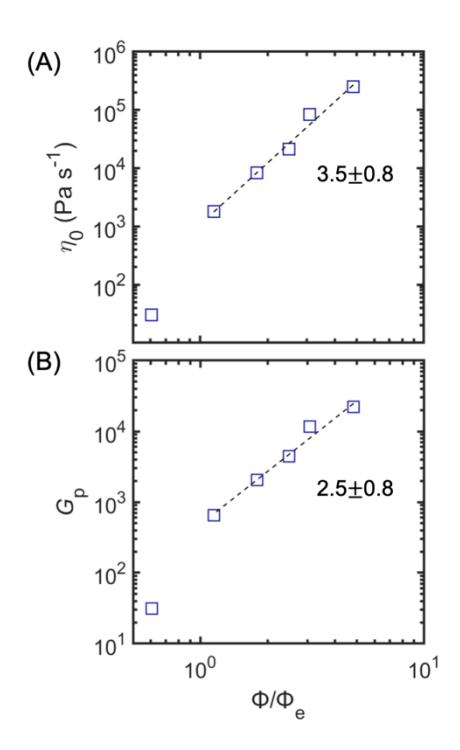
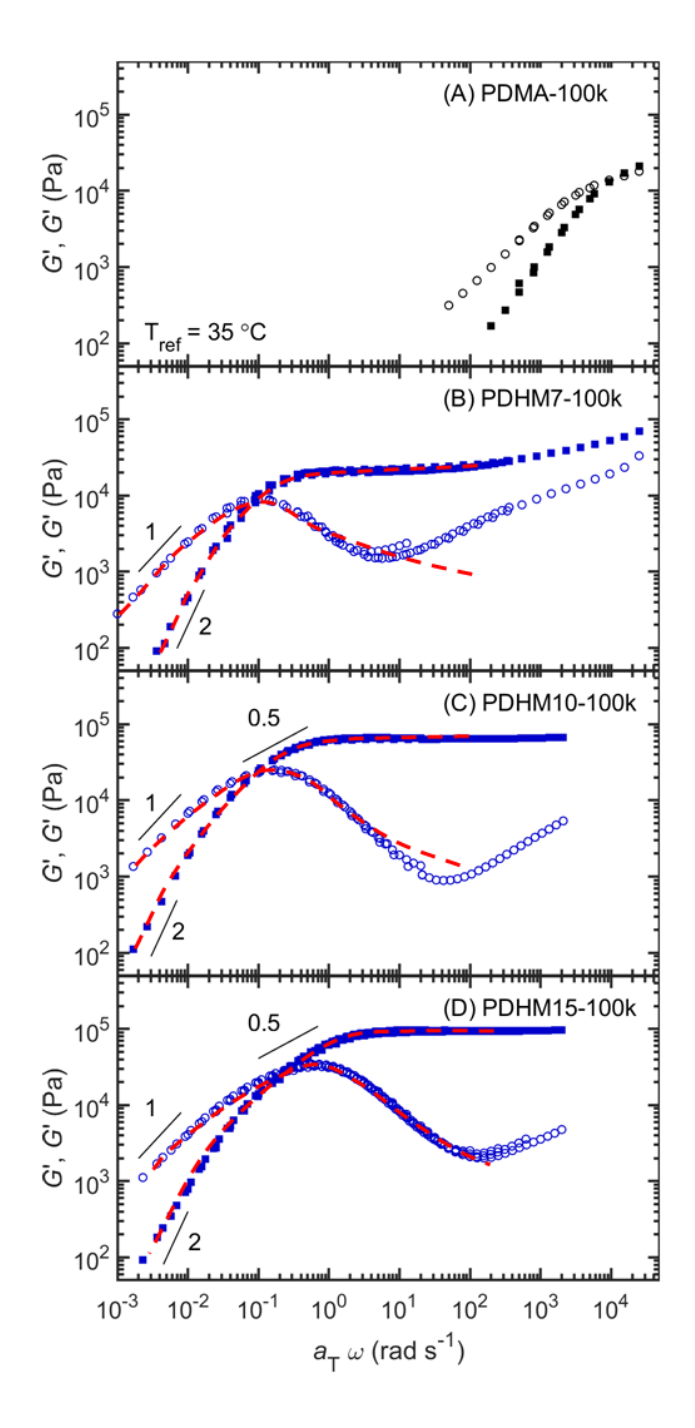


Figure 3. (a) Plot of the zero shear viscosity,  $\eta_0$ , as a function of concentration,  $\phi/\phi_e$ , for PDHM7-100k measured at 35 °C. Dashed lines show power law fit for concentrations that are above the entanglement concentration ( $\phi > \phi_e$ ). (b) Plot of the high-frequency plateau modulus,  $G_p$ , as a function of concentration,  $\phi/\phi_e$ , for PDHM7-100k measured at 35 °C.

The effect of entanglements on viscoelastic response is enhanced at higher network sticker density compared to those with 7 stickers per chain, as revealed by a comparison of gels with different sticker densities but constant chain length and concentration. Frequency sweeps were performed on additional polymers with 0, 10 and 15 stickers per chain, each with a molar mass of ~100 kg mol<sup>-1</sup> (denoted PDMA-100k, PDHM10-100k and PDHM15-100k). All samples were prepared at 4.8  $\phi_e$  and the measurements were performed at temperatures ranging from T = 5 – 55 °C. Time-temperature superposition (TTS) was then used to plot the data as G' and G'' vs  $\omega a_T$ , as shown in Figure 4, with 35 °C set as the reference temperature,  $T_{\text{ref}}$ . The concentration of  $\phi = 4.8\phi_e$  chosen for this analysis is larger than those studied by self-diffusion measurements to more

clearly determine the effect of entanglements on the scalings of G' and G'' with frequency. The results of this analysis will be used to estimate the extent of entanglement for the concentrations investigated for the self-diffusion studies.



**Figure 4.** Plot of G' (filled symbols) and G'' (unfilled symbols) vs  $\omega$  for (A) PDMA-100k (B) PDHM7-100k (C) PDHM10-100k and (D) PDHM15-100k all prepared at 4.8  $\phi_e$ . Experiments

were performed at 5 – 55 °C and TTS was used to plot G' and G'' vs  $\omega a_T$ , with  $T_{ref} = 35$  °C. The dashed red lines are fits to the sticky double reptation model<sup>28</sup> (see Figures S7–S9 for comparison to fits with a single Maxwell mode).

The presence of entanglements in the PDHM gels of various sticker densities is seen in Figure 4 as a slight but noticeable broadening of the relaxation spectrum following the initial drop in G' from the high-frequency plateau. As the number of stickers per chain is increased from 7 to 15, the broadening becomes more apparent, with G' showing a slope of  $\sim$ 0.5 before entering the terminal regime with a scaling of  $\sim$ 2, as most clearly seen for the PDHM15-100k gel (Figure 4d). For the loss modulus, G'', a minimum is seen at higher frequencies followed by a maximum close to (but not exactly at) the crossover frequency, with a scaling of  $\sim$ 0.5 before transitioning into the terminal regime with slope of  $\sim$ 1. While similar features are seen in the PDHM10-100k gel (10 stickers/chain), these features are not as apparent for the PDHM7-100k gel (7 stickers/chain). However, for all sticker densities, the presence of cross-links in the network drastically delays the terminal relaxation by several orders of magnitude compared to an uncrosslinked network of identical chain molecular weight (i.e., without metal-coordinating groups), for which terminal relaxation occurs at  $\omega$  > 100 rad s<sup>-1</sup> as shown in Figure 4a.

The data shown in Figure 4 are consistent with models for entangled associative networks proposed by Chen *et al.* (sticky double reptation: SDR model)<sup>28</sup> and Ahmadi *et al.* (hindered fluctuation: HF model)<sup>18</sup>. Both the SDR and the HF model are modified forms of the sticky reptation model<sup>42</sup> originally proposed by Rubinstein and Semenov, in which chain relaxation can occur when either of the two chains forming the entanglement diffuses away. The HF model also

includes the effects of contour length fluctuations (CLF), but this results in only minor changes to the predicted frequency sweeps as in some cases the effects of CLF are too fast to be seen. In the absence of CLF effects, their predictions are qualitatively similar to the SDR model. Fits to the SDR model show reasonable agreement for the data on the PDHM-100k gels of all sticker densities at a concentration of  $\phi = 4.8\phi_e$ , suggesting that the effects of CLF are too fast to be observed in these gels. Fits were performed using the RepTate software package<sup>37</sup> and are shown as dashed red lines in Figure 4, with the fit parameters listed in Table 1, including the effective number of stickers per chain  $(n_s)$ , effective number of entanglements per chain  $(n_e)$ , and sticky bond lifetime  $(\tau_s)$ . Note that although the sticker chemistry is identical for all the gels studied, the sticker lifetime  $\tau_s$  was allowed to vary to allow for minor variations in the local sticker environment at each sticker density; as shown in Table 1, the values of  $\tau_s$  for all cases are equal (to within their uncertainties), consistent with the identical network chemistry used in all systems. In both the SDR and HF models, the plateau modulus  $G_p$  has contributions from both the stickers and entanglements, except in the low-sticker-density limit where  $G_p$  is expected to show contributions only from entanglements. The frequency sweep is expected to show different features for each case.

For associative networks where the viscoelastic properties show contributions only from the entanglements (usually seen at low sticker density), both the SDR and HF models predict that only a single relaxation time will be observed corresponding to the inverse of the crossover frequency (i.e.,  $\tau = 1/\omega_c$ ). This relaxation time should be much longer in the gel than in the corresponding non-associative polymer solution. These predictions are consistent with the frequency sweep seen for the low-sticker-density systems PDHM7-100k (7 stickers per chain) and PDMA-100k (no stickers), with the PDHM7-100k gel having a significantly longer relaxation time than the uncrosslinked PDMA-100k gel (i.e.,  $\tau_{\text{rep}, PDHM7-100k} >> \tau_{\text{rep}, PDMA-100k}$ ; see **Table 1**). This

result is supported by the concentration dependence of the plateau modulus of  $G_p \sim \phi^{2.5\pm0.8}$  found for the PDHM7-100k gels (Figure 3b), which is close to the predicted scaling for a non-associative entangled polymer solution  $(G_p \sim \phi^{2.25})$ . It should be noted that the sticky reptation models apply rigorously in the limiting case of long chains with many stickers and entanglements per chain; the PDHM7-100k gels studied here have relatively few stickers per chain and are in the weakly entangled regime.

For systems in which  $G_P$  has contributions from both the entanglements and stickers, the frequency sweep is expected to show additional relaxation processes arising from the interplay of binding and topological confinement.<sup>18, 28</sup> For the higher-sticker-density gels (PDHM10-100k and PDHM15-100k), following the initial drop in the high-frequency plateau modulus, a broadening in the relaxation profile is observed with both G' and G'' having log-log slopes of  $\sim$ 0.5. This broadening, which is attributed to sticky Rouse relaxation by both the SDR and HF models,<sup>18, 28</sup> shows a slight increase at higher sticker density. Finally, at frequencies below the crossover frequency, both G' and G'' show terminal power-law scalings of  $\sim$ 2 and  $\sim$ 1 respectively. The inverse of the frequency at which the terminal regime occurs corresponds to the longest relaxation time,  $\tau_{rep}$ , of the gel.<sup>18, 24, 28</sup>

**Table 1.** The values of plateau modulus  $G_p$  (in the region  $10^0 < a_T \omega < 10^2$ ), number of active stickers per chain  $n_s$ , number of active entanglements per chain  $n_e$ , effective bond  $\tau_s$ , and terminal relaxation time  $\tau_{rep}$  for PDMA-100k, PDHM7-100k, PDHM10-100k and PDHM15-100k, at T = 35 °C. <sup>a</sup>

Polymer	$G_{\rm p}({ m kPa})$	$n_{\rm s}$	$n_e$	$\tau_s$ (s)	$ au_{rep}$ (s)
PDMA-100k	21.2 в	-	~ 4.9 °	-	6 × 10 <sup>-4 b</sup>

PDHM7-100k	21.7 b	$3\pm9$ d	$2\pm7^{d}$	$5 \pm 25$ d	70 °
PDHM10-100k	63.6 b	7 ± 2 <sup>d</sup>	$2.8 \pm 0.5$ d	2 ± 2 <sup>d</sup>	305 °
PDHM15-100k	95.5 b	10 ± 2 <sup>d</sup>	$3.5 \pm 0.3$ d	$1.0 \pm 0.4$ d	347 °

<sup>&</sup>lt;sup>a</sup>  $G_p$  is the plateau modulus,  $n_s$  is the number of stickers per chain,  $n_e$  is the number of entanglements per chain,  $\tau_s$  is the sticker lifetime and  $\tau_{rep}$  is the reptation time. <sup>b</sup> Values obtained from frequency sweeps in Figure 4. <sup>c</sup> Estimated using eq. 1 and  $N_{e,0}$  from ref. <sup>34 d</sup> Fit parameters from fits to the SDR model. <sup>e</sup> Calculated from  $n_s$ ,  $n_e$  and  $\tau_s$  via  $\tau_{rep} = \tau_s n_e n_s^2$ .

The values of  $n_s$ ,  $n_e$  and  $\tau_s$  obtained from fits to the SDR model show reasonable agreement with the known properties of the PDHM-100k gels (see **Table 1**). The values of the number of active stickers per chain,  $n_s$ , in **Table 1** are smaller than the sticker density S determined by  $^1$ H NMR, indicating that only a fraction of the stickers are elastically active as intermolecular bonds at a given time. The remaining stickers may either exist as intrachain bonds or in the dissociated state (see **Figure 1**b). Given that the values of the sticker lifetime,  $\tau_s$ , are similar (within the error of the measurement) to the Ni<sup>2+</sup>-bis(histidine) bond lifetime reported in the same gel environment of  $\tau_s \approx 5$  s,<sup>35</sup> it appears that the bond lifetime renormalization as described in the sticky Rouse model<sup>23,26</sup> is not a significant effect in this system. In particular, the network relaxation times  $\tau_s$  obtained from the crossover frequency in shear rheology (i.e.,  $\tau_s \approx 1/\omega_c$ ) for the previously reported unentangled PDHMS-25k gels<sup>31</sup> are larger than the effective bond lifetimes  $\tau_s$  reported here by a factor of ~10, consistent with a minimal contribution from bond renormalization in the gels studied here.

Finally, the number of entanglements per chain,  $n_e$ , for the PDHM-100k gels at the concentration corresponding to 4.8  $\phi_e$  is found to be ~2 - 3.5, in approximate agreement with the value of 4.9 estimated for PDMA-100k based on the literature.<sup>34</sup> The presence of sticker

associations is hypothesized to reduce a chain's pervaded volume due to the formation of intramolecular bonds (i.e., loops), 33,43 which in turn would reduce the extent of chain entanglement compared to chains of identical molecular weight but without associative groups. This is consistent with the lower values of  $n_e$  determined for the PDHM-100k gels compared to estimates for the non-associative PDMA-100k precursor at this concentration. The transition from the unentangled to the weakly entangled regime for non-associative polymers is expected to occur at ~2 entanglements per chain. Thus, the values of  $n_e$  obtained from the fits are consistent with a transition from the unentangled to the weakly entangled regime. Based on the results for all sticker densities probed and using a concentration scaling of  $n_e \sim \phi^{1.3}$  obtained from Ref.<sup>42</sup>, the number of entanglements per chain for the PDHM7-100k gels at the concentrations investigated in selfdiffusion measurements ( $\phi/\phi_e = 1.1$ , 1.8, 2.5, and 3.1) are estimated as  $n_e = 0.7$ , 1.1, 1.5 and 1.9, respectively. The estimation of  $n_e$  solely based on the data for the PDHM7-100k gels (Figure 2) would have been prone to larger error as shown by the error associated in the fit parameters for PDHM7-100k gel in **Table 1**. This further shows the subtle nature of the effects of entanglements on the macroscopic rheological behavior of the network, highlighting the importance of other techniques that are more sensitive to the changes occurring in the transition from the unentangled to the weakly entangled regime.

Self-diffusion above the concentration for entanglement. Self-diffusion of the network-forming chains in the entangled PDHM-100k gels of various concentrations was measured using forced Rayleigh scattering (FRS). Due to the dynamic range of FRS, the self-diffusion measurements were performed on gels with 7 stickers per chain (PDHM7-100k) at concentrations of  $1.1-3.1\phi_e$ . Note that other sticker densities were not investigated using FRS since their self-diffusion time scales were not experimentally accessible. In contrast to the relatively mild effects

on the frequency sweep measurements (see Figures 2 and 4), the presence of entanglements imparts a strong qualitative transition in the self-diffusive behavior of the PDHM7-100k gels, specifically in the extent of apparent superdiffusive scaling on length scales smaller than the terminal Fickian limit. For gel concentrations of 1.1 to 2.5  $\phi_e$ , apparent superdiffusive scaling is observed on small length scales ( $d^2 = 0.2 - 10 \, \mu m^2$ ) followed by a transition to terminal Fickian diffusion on long length scales ( $d^2 > 10 \, \mu m^2$ ). As in previous work, however, it is important to note that even the smallest length scales probed by FRS are several times greater than the chain radius of gyration. The extent of superdiffusive scaling is indicated by the width of the apparent superdiffusive regime, which decreases with concentration such that the transition to Fickian scaling shifts to lower values of  $d^2$ . Finally, at the highest concentration investigated ( $\phi = 3.1\phi_e$ ), superdiffusive scaling is not observed, and gels exhibit only Fickian scaling on all length scales within the accessible range of the instrument.

The observation of superdiffusive scaling that transitions to a Fickian scaling regime has been seen in other measurements of self-diffusion using FRS, but only in associative networks in the unentangled regime ( $\phi < \phi_e$ ).<sup>29-31</sup> These measurements include a recent study involving the same backbone and sticker chemistry of poly(N, N-dimethylacrylamide) with pendant histidine side groups, with sticker densities of S = 5 - 15 and molar mass of around 25,000 g/mol (which will be referred to as PDHMS-25k to distinguish it from the polymers in this study).<sup>31</sup> For these unentangled polymers, the two diffusive modes seen by FRS have been suggested to arise from molecular walking and hopping.<sup>32, 33</sup> The qualitative similarities between the diffusive regimes seen for the entangled PDHM-100k gels and the unentangled PDHMS-25k gels studied previously suggest that the same dynamic modes play an important role in chain self-diffusion even in the weakly entangled regime as probed here.

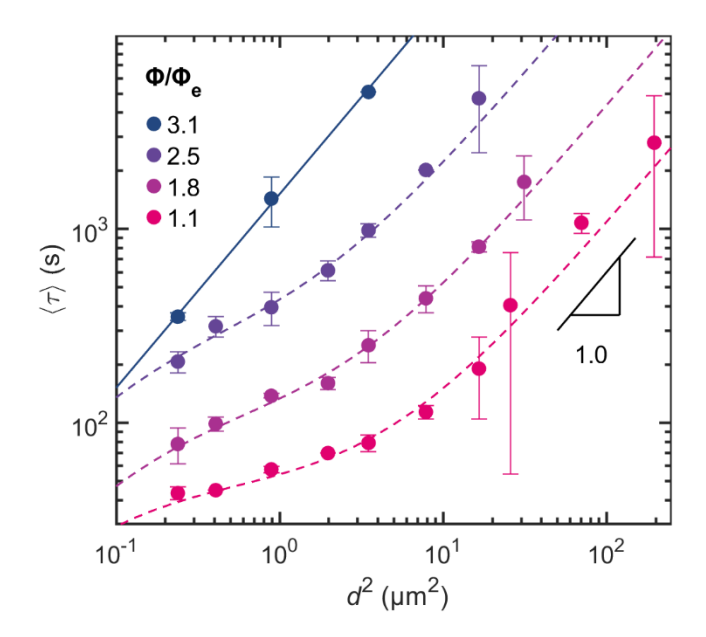


Figure 5. Plot of  $\langle \tau \rangle$  vs  $d^2$  for PDHM7-100k at 1.1-3.1  $\phi_e$  (which corresponds to 10-28 vol%), measured at 35 °C. The dashed lines are fits to the two-state model while the solid line is a linear regression to determine the diffusivity of the sample at 3.1  $\phi_e$ . Error bars represent standard error of measurements that were performed in triplicate.

Origin of superdiffusive scaling in weakly entangled networks. The previously proposed two-state model<sup>29</sup> was used to analyze the self-diffusion data for the studies of various unentangled associative networks showing superdiffusive scaling and is able to capture the self-diffusion data for all except the highest concentration gels studied here (i.e.,  $\phi = 1.1 - 2.5\phi_e$ , as shown by the dashed lines in Figure 5). The two-state model is a semi-empirical model that hypothesizes that the network-forming chains exist in two apparent states with distinct diffusivities,  $D_A$  and  $D_M$  (units:  $\mu$ m s<sup>-1</sup>), where  $D_A \ll D_M$ . The two apparent states are hypothesized to be (1) an associated state (with diffusivity  $D_A$ ) which is connected to the network and may undergo relatively slow diffusion by single-chain walking or cooperative motion of multi-chain bound clusters, and (2) a molecular state (with diffusivity  $D_M$ ) which consists of single molecules

or small clusters that are transiently disconnected from the network and may undergo relatively fast diffusion by hopping. The polymers can interconvert between the two states with interconversion rates,  $k_{\rm on}$  and  $k_{\rm off}$  (units: s<sup>-1</sup>), with pseudo-first order kinetics. Since the physical details of the two diffusive states are not specified in the model, the model can be applied for the entangled PDHM7-100k gels without modification, with the molecular identities of the two diffusive states assumed to be qualitatively equal as in unentangled systems. The associated state (i.e., walking) diffusivity  $D_A$  can be related to the chain's orientational relaxation time as governed by strand exchange. 32, 33 It is important to note that the parameters  $k_{\rm on}$  and  $k_{\rm off}$  are not intended to represent physical rate constants but rather an effective interconversion rate between the two apparent species. While the probability of complete dissociation of a single chain from the network can in principle be estimated from the equilibrium constant  $K_{eq}$  and the sticker density,<sup>29</sup> it is difficult to estimate the contribution of the hopping mode solely from knowledge of the hopping probability, as it is convoluted by the presence of loops and also depends on the relative rate of bound-state (i.e., walking) diffusion. Thus, while the effective diffusivities and rate constants in the two-state model are functions of molecular features such as the number of stickers per chain and molecular weight (and may vary in entangled vs unentangled systems, as well as in hydrogels vs melts), the two-state model does not specify a direct relationship between them as in the sticky Rouse and reptation models.  $^{18, 28, 42}$  In addition, the individual model parameters  $D_A$ ,  $D_M$ ,  $k_{on}$  and  $k_{\rm off}$  cannot be independently determined, as shown previously.<sup>29</sup> However, the parameters of relevance are the effective diffusivity in the large length-scale Fickian regime, given by  $D_{M,eff}$  $D_M/(1+K_{eq})$  and the extent of anomalous diffusion,  $\gamma K_{eq} = D_A/D_M \cdot k_{on}/k_{off}$ , which is the ratio of the diffusivities of the two modes weighted by their relative populations. Note that  $\gamma K_{eq}$ 

can take any value between 0 and 1 and is inversely proportional to the width of the apparent superdiffusive regime in logarithmic-space.

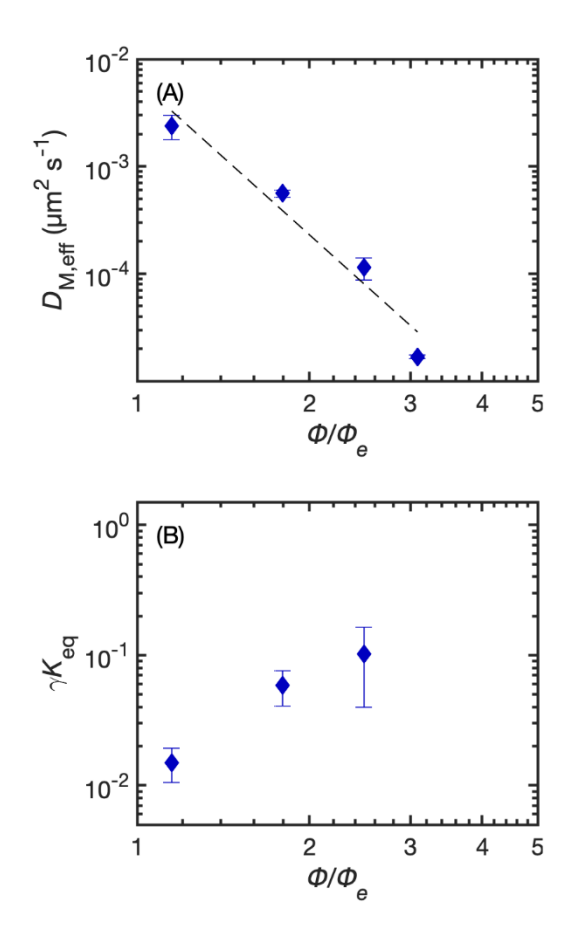


Figure 6. Effect of concentration on (A) the effective diffusivity in the large length-scale Fickian regime,  $D_{M,eff}$ , and (B) the extent of anomalous diffusion  $\gamma K_{eq}$  for gels of PDHM7-100k (~7 stickers per chain). The parameters were obtained by fitting the analytical solution of the two-state model to the experimentally derived relation  $\langle \tau \rangle$  vs  $d^2$  for gels at  $1.1 - 2.5 \phi_e$ . In panel A, the dashed line is a power-law fit to the data to obtain a scaling relation of  $D_{M,eff} \sim \phi^{-5\pm 1}$ .

Even when accounting for differences in the chain lengths and sticker spacings (N and l, respectively), the long-time effective diffusivities  $D_{M,eff}$  reported here for the PDHM7-100k gels (7 stickers per chain) are ~4 orders of magnitude smaller than the  $D_{M,eff}$  values measured

previously<sup>31</sup> for the unentangled associative PDHMS-25k gels with 5-15 stickers per chain (see Figure S10). This provides strong evidence that self-diffusion in the entangled PDHM7-100k gels is hindered by additional barriers to diffusion beyond the effect of the stickers alone. The effective diffusivity in the long-time Fickian regime,  $D_{M,eff}$  decreases with concentration with a power-law scaling of  $D_{M,eff} \sim \phi^{-5\pm 1}$  (Figure 6a), indicating increased hindrance to diffusion at higher concentrations, though the limited accessible concentration range of less than half a decade precludes conclusive quantification of this power-law exponent. Since the number of entanglements per chain in the gels here ranges from  $n_e = 0.7 - 1.9$ , these gels are expected to span the transition between the sticky Rouse and sticky reptation models, which apply in the limits of unentangled and entangled gels, respectively.<sup>23, 26</sup> While these mean-field models do not consider the existence of multiple diffusive modes, the physics presented in these models should apply in the long-time Fickian regime observed in Figure 5, and as such can be compared with the  $D_{
m M,eff}$  values in Figure 6. For gels that are below the entanglement limit ( $n_e < 1$ ) in a good solvent (Flory exponent  $\nu = 0.588$ ), the sticky Rouse model predicts a diffusivity scaling law of  $D \sim \phi^{-0.4}$ while above the entanglement concentration  $(n_e > 1)$  the sticky reptation model predicts  $D\sim\phi^{-1.69}$ . For the gels investigated in this work, the scaling exponent of  $-5\pm1$  is a significantly stronger dependence than predicted in either regime. A similarly strong concentration dependence has previously been observed in associative protein self-diffusion<sup>29, 44</sup> and here may arise from a crossover between the limiting regimes treated theoretically. It is also worth noting that the sticky reptation model assumes that gels are in the well entangled regime where there are many entanglements per chain ( $\phi > 4\phi_e$ ), and thus the predictions of the model may not strictly apply to the results reported here.

The decrease in the width of the superdiffusive scaling regime with increasing concentration (equivalently, extent of entanglement) is further reflected by the increase of  $\gamma K_{eq}$ with concentration. Since  $\gamma K_{eq}$  can be recast as  $\gamma K_{eq} = \frac{D_A}{D_{M,eff}}$ , increasing  $\gamma K_{eq}$  can be interpreted as a convergence between the effective diffusivity in the Fickian regime,  $D_{M,eff}$ , and the diffusivity of the slow (i.e., associated) state,  $D_A$ . In the two-state model, pure Fickian diffusion is recovered when the diffusivities of the mobile and associated states are equal. This reduction in the width of the superdiffusive regime is seen in Figure 5 with increasing concentration as the contribution of the mobile state to the overall diffusivity is reduced. At the highest concentration probed ( $\phi = 3.1\phi_e$ ), the diffusive rates converge such that only one apparent diffusive species is observed, resulting in purely Fickian scaling on all length scales. It is important to note that the widths of the superdiffusive regimes observed here are also significantly smaller than those observed for all the conditions investigated for the unentangled PDHMS-25k gels. This is seen from Figure 6b where the value of  $\gamma K_{eq}$  range from  $10^{-2}$  to  $10^{-1}$  for the entangled gels here, while the values of  $\gamma K_{eq}$  for the PDHMS-25k gels ranged from  $10^{-4}$  to  $10^{-3}$  for the unentangled gels.<sup>31</sup> For the unentangled PDHMS-25k gels, superdiffusive scaling was seen for gels with as many as 15 stickers per chain, which indicates that an increase in the effective diffusivity due to hopping in the PDHM gels is possible in the absence of entanglements, even at high sticker density. In the presence of entanglements, however, a chain in the PDHM7-100k gels would not only have to dissociate all its stickers from the network, but it would also have to release itself from entanglements in order to diffuse by hopping over length scales greater than  $R_g$ . Thus, the value of  $\gamma K_{eq}$  increasing from 0.01 to 1 (i.e., a suppression of apparent superdiffusive scaling) for the PDHM7-100k gels provides evidence of a transition point where the presence of entanglements

prevents the polymers from undergoing appreciable diffusion from hopping, resulting in walking being the only diffusive mode present in the system.

While little experimental data on self-diffusion in entangled associative gels has been reported to date, the presence of two diffusive modes with diffusivities that differ by 2-4 orders of magnitude in entangled, hydrogen bonding melts has previously been reported by Jangizehi et  $al..^{20,45}$  In their work, they studied associative networks with 0.3-11 entanglements per chain and 0 - 20 stickers per chain, using fluorescence recovery after photobleaching (FRAP). In their unentangled sample (number of stickers per chain  $N_s = 1$ , number of entanglements per chain  $n_e =$ 0.3), the two dynamic modes were found to have diffusivities of the order of  $10^{-1}$  and  $10^{1}$  µm<sup>2</sup> s<sup>-1</sup>. Above the entanglement threshold ( $N_s = 13$ ,  $n_e = 4.1$ ), the two diffusivities drop to the order of  $10^-$ <sup>4</sup> and  $10^{-1} \, \mu \text{m}^2 \, \text{s}^{-1}$ . Finally, in their highly entangled systems ( $N_s = 12, N_e = 11$ ) the diffusivity is dominated by a single mode with  $D \sim 10^{-5} \ \mu m^2 \ s^{-1}$ . Their reported diffusivities are similar to the values of the slow mode  $D_A$  (10<sup>-5</sup>  $\mu$ m<sup>2</sup> s<sup>-1</sup>) and the fast mode  $D_M$  (10<sup>0</sup>  $\mu$ m<sup>2</sup> s<sup>-1</sup>) in the PDHM-100k gels studied here (see Figure S5). However, for the entangled hydrogen-bonding melts, Jangisehi et al. attributed the fast and slow diffusive modes to the relaxation of, respectively, binary hydrogen-bonding associations and long-lived phase-separated clusters of multiple hydrogenbonding groups. In particular, phase-separated clusters were hypothesized to be present in the hydrogen-bonded melts due to a significant broadening in their frequency sweep profiles, resulting in an experimentally inaccessible terminal relaxation regime.<sup>20</sup> In contrast, the terminal relaxation regime for the PDHM gels studied here is accessible for all concentrations and sticker densities probed (see Figures 2 and 4), suggesting the absence of such long-lived phase-separated domains in these gels. Thus, the two diffusive modes observed in the FRS measurements are assigned as molecular hopping and walking, similar to the unentangled PDHMS-25k gels studied previously.<sup>31</sup>

Comparison of the time scales from self-diffusion and linear viscoelastic measurements. The complementary timescales of chain motion as probed by shear rheology and self-diffusion studies can be related via the scaling argument

$$\tau \approx \frac{R_g^2}{D_{M,eff}} \tag{5}$$

where  $\tau$  is the characteristic chain relaxation time,  $D_{M,eff}$  is the long-time effective diffusion coefficient (corresponding to the terminal slopes of Fig. 5), and  $R_g \approx bN^{0.5}\phi^{-0.115}$  is the chain radius of gyration in semi-dilute conditions in a good solvent, as in the gels studied here (for PDMA,  $N \approx 170^{-34}$  and b = 1.4 nm  $^{46}$ ). Comparing the self-diffusion timescales determined using Eq. 5 with the characteristic network relaxation times indicated by the cross-over of G' and G'' in frequency sweep measurements ( $\tau \approx 1/\omega_c$  with  $\omega_c$  being the crossover frequency where G' = G'') at different concentrations allows for a comparison of the dynamic modes probed by the two measurements. As seen in Figure 7, both relaxation timescales increase with concentration, as expected. However, the relaxation times from self-diffusion have a stronger concentration dependence than those from rheology. The difference in the concentration dependencies of the two relaxation times is consistent with prior studies of the unentangled PDHMS-25k gels<sup>31</sup> (see Figure S11). However, for the entangled gels studied here, due to their different concentration dependencies, the timescales from rheology and self-diffusion appear to converge with increasing concentration until they become approximately equal at the highest concentration of  $\phi = 3.1\phi_e$ .

The convergence of the two timescales shown in Figure 7 correlates with the reduction in superdiffusive behavior with increasing concentration as shown in Figure 5. At the highest concentration of  $\phi = 3.1\phi_e$ , the corresponding self-diffusion and rheological relaxation times are approximately equal, while only Fickian scaling is observed in the self-diffusion measurements.

This suggests a link between the presence of the fast diffusion mode (e.g., hopping), which leads to apparent superdiffusive scaling and determines the long-time self-diffusivity  $D_{M,eff}$ , and may contribute to the difference in the timescales probed by the two measurements. The differing diffusive and rheological timescales represent a substantial unsolved puzzle in understanding the fundamental behavior of these dynamic networks.

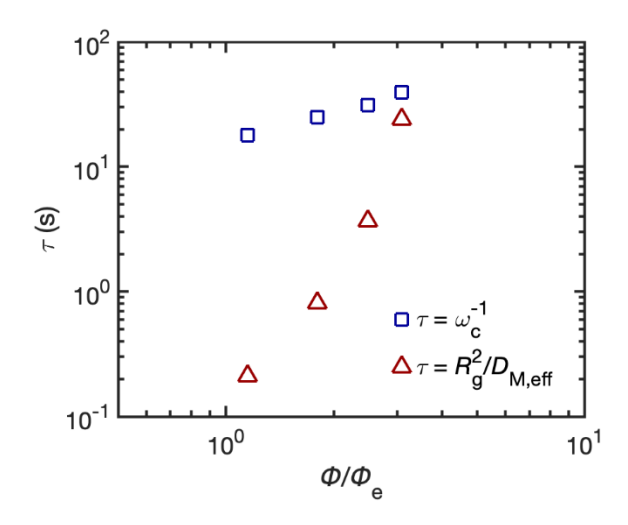


Figure 7. Plot of  $\tau$  as a function of concentration,  $\phi/\phi_e$ , with  $\tau=1/\omega_c$  from frequency sweep measurements and  $\tau=R_g^2/D_{M,eff}$  from self-diffusion measurements.

# Conclusion

This work investigated the transition from the unentangled to the weakly entangled regime in physically associative networks, using model hydrogels comprising a linear random copolymer of N,N-dimethylacrylamide and a histidine-functionalized monomer crosslinked with Ni<sup>2+</sup> ions. Viscoelastic properties investigated by shear rheology are consistent with a transition from the unentangled to the weakly entangled regime, with an estimated number of entanglements per chain of  $\sim 0.7-2.0$  for the PDHM7-100k gels containing  $\sim 7$  stickers per chain at concentrations ranging from 1.1-3.1  $\phi_e$ . The concentration dependence of the zero-shear viscosity and reptation time

show qualitative agreement with the predicted scaling in the sticky reptation model, demonstrating the presence of entanglements in the overall network relaxation behavior.

Further study of the self-diffusive behavior of the network-forming chains revealed a strong effect of entanglements in suppressing diffusion by molecular "hopping," resulting in a suppression of apparent superdiffusive scaling up to a limit of purely Fickian scaling on all length scales for the highest concentration probed ( $\phi = 3.1\phi_e$ ). The observation of apparent superdiffusive scaling at lower concentration ( $\phi < 3.1\phi_e$ ) indicates the presence of two diffusive modes with distinct diffusivities, which has been previously reported in several different associative networks in the unentangled regime. In the unentangled gels, the two modes were assigned to be walking and hopping; thus, the transition to purely Fickian scaling at 3.1  $\phi_e$  in the gels here suggests a complete suppression of the hopping mode due to entanglements, such that self-diffusion occurs by walking alone on all length scales. In addition, a comparison of the selfdiffusion timescales with the strand exchange timescales measured by rheology demonstrates a convergence between the two timescales with increasing concentration, further suggesting a reduced presence of hopping with increasing concentration. Overall, the combination of shear rheology and forced Rayleigh scattering provides complementary insights into chain dynamics in entangled associative networks, with implications for their design for applications spanning biomedicine, soft robotics, and self-healing materials.

#### ASSOCIATED CONTENT

The Supporting Information is available at [link inserted by publisher]

Supplementary figures and tables; scaling relationships of the effective diffusivity with respect to *N* and *l*; and representative forced Rayleigh scattering decay curves and their associated fits.

#### **AUTHOR INFORMATION**

#### **Corresponding Author**

\*(N.H-A) Email holten@mit.edu

\*(B.D.O) Email bdolsen@mit.edu

#### Notes

The authors declare no competing financial interest.

#### ACKNOWLEDGMENT

This work was supported in part by the MRSEC Program of the National Science Foundation under award number DMR - 1419807, the National Science Foundation under Award DMR-1709315, the U.S. Army Research Office through the Institute for Soldier Nanotechnologies under Contract W911NF-07-D-0004 and the Office of Naval Research (ONR) under the Young Investigators Program Grant ONR.N00014-15-1-2763. A.R. acknowledges support from the Department of Defense through a National Defense Science and Engineering Graduate Fellowship.

### References

- 1. Li, C. H.; Wang, C.; Keplinger, C.; Zuo, J. L.; Jin, L.; Sun, Y.; Zheng, P.; Cao, Y.; Lissel, F.; Linder, C.; You, X. Z.; Bao, Z., A highly stretchable autonomous self-healing elastomer. *Nat Chem* **2016**, *8* (6), 618-24.
- 2. Tee, B. C.; Wang, C.; Allen, R.; Bao, Z., An electrically and mechanically self-healing composite with pressure-and flexion-sensitive properties for electronic skin applications. *Nature nanotechnology* **2012**, *7* (12), 825.
- 3. Sanoja, G. E.; Schauser, N. S.; Bartels, J. M.; Evans, C. M.; Helgeson, M. E.; Seshadri, R.; Segalman, R. A., Ion Transport in Dynamic Polymer Networks Based on Metal–Ligand Coordination: Effect of Cross-Linker Concentration. *Macromolecules* **2018**, *51* (5), 2017-2026.

- 4. Zhang, Q.; Niu, S.; Wang, L.; Lopez, J.; Chen, S.; Cai, Y.; Du, R.; Liu, Y.; Lai, J. C.; Liu, L., An Elastic Autonomous Self-Healing Capacitive Sensor Based on a Dynamic Dual Crosslinked Chemical System. *Advanced Materials* **2018**, *30* (33), 1801435.
- 5. Bode, S.; Zedler, L.; Schacher, F. H.; Dietzek, B.; Schmitt, M.; Popp, J.; Hager, M. D.; Schubert, U. S., Self-healing polymer coatings based on crosslinked metallosupramolecular copolymers. *Advanced Materials* **2013**, *25* (11), 1634-1638.
- 6. Scheltjens, G.; Diaz, M.; Brancart, J.; Van Assche, G.; Van Mele, B., A self-healing polymer network based on reversible covalent bonding. *Reactive and Functional Polymers* **2013**, 73 (2), 413-420.
- 7. Glassman, M. J.; Olsen, B. D., Structure and mechanical response of protein hydrogels reinforced by block copolymer self-assembly. *Soft matter* **2013**, *9* (29), 6814-6823.
- 8. Guvendiren, M.; Lu, H. D.; Burdick, J. A., Shear-thinning hydrogels for biomedical applications. *Soft matter* **2012**, *8* (2), 260-272.
- 9. Wever, D.; Picchioni, F.; Broekhuis, A., Polymers for enhanced oil recovery: a paradigm for structure–property relationship in aqueous solution. *Progress in Polymer Science* **2011**, *36* (11), 1558-1628.
- 10. Taylor, K. C.; Nasr-El-Din, H. A., Water-soluble hydrophobically associating polymers for improved oil recovery: A literature review. *Journal of Petroleum Science and Engineering* **1998**, *19* (3-4), 265-280.
- 11. Zhao, X., Multi-scale multi-mechanism design of tough hydrogels: building dissipation into stretchy networks. *Soft matter* **2014**, *10* (5), 672-687.
- 12. Shen, W.; Zhang, K.; Kornfield, J. A.; Tirrell, D. A., Tuning the erosion rate of artificial protein hydrogels through control of network topology. *Nature materials* **2006**, *5* (2), 153-158.
- 13. Shen, W.; Lammertink, R. G.; Sakata, J. K.; Kornfield, J. A.; Tirrell, D. A., Assembly of an artificial protein hydrogel through leucine zipper aggregation and disulfide bond formation. *Macromolecules* **2005**, *38* (9), 3909-3916.
- 14. Petka, W. A.; Harden, J. L.; McGrath, K. P.; Wirtz, D.; Tirrell, D. A., Reversible hydrogels from self-assembling artificial proteins. *Science* **1998**, *281* (5375), 389-392.
- 15. Tang, S.; Glassman, M. J.; Li, S.; Socrate, S.; Olsen, B. D., Oxidatively Responsive Chain Extension to Entangle Engineered Protein Hydrogels. *Macromolecules* **2014**, *47* (2), 791-799.
- 16. Cao, P. F.; Li, B.; Hong, T.; Townsend, J.; Qiang, Z.; Xing, K.; Vogiatzis, K. D.; Wang, Y.; Mays, J. W.; Sokolov, A. P., Superstretchable, self-healing polymeric elastomers with tunable properties. *Advanced Functional Materials* **2018**, *28* (22), 1800741.
- 17. Ahmadi, M.; Jangizehi, A.; van Ruymbeke, E.; Seiffert, S., Deconvolution of the Effects of Binary Associations and Collective Assemblies on the Rheological Properties of Entangled Side-Chain Supramolecular Polymer Networks. *Macromolecules* **2019**, *52* (14), 5255-5267.
- 18. Ahmadi, M.; Hawke, L. G. D.; Goldansaz, H.; van Ruymbeke, E., Dynamics of Entangled Linear Supramolecular Chains with Sticky Side Groups: Influence of Hindered Fluctuations. *Macromolecules* **2015**, *48* (19), 7300-7310.
- 19. Hawke, L. G. D.; Ahmadi, M.; Goldansaz, H.; van Ruymbeke, E., Viscoelastic properties of linear associating poly(n-butyl acrylate) chains. *Journal of Rheology* **2016**, *60* (2), 297-310.
- 20. Jangizehi, A.; Ghaffarian, S. R.; Schmolke, W.; Seiffert, S., Addition to "Dominance of Chain Entanglement over Transient Sticking on Chain Dynamics in Hydrogen-Bonded Supramolecular Polymer Networks in the Melt". *Macromolecules* **2019**, *53* (1), 491-493.
- 21. Seiffert, S.; Sprakel, J., Physical chemistry of supramolecular polymer networks. *Chem Soc Rev* **2012**, *41* (2), 909-30.

- 22. Baxandall, L.; Edwards, S., Deformation-dependent properties of polymer networks constructed by addition of crosslinks under strain. *Macromolecules* **1988**, *21* (6), 1763-1772.
- 23. Rubinstein, M.; Semenov, A. N., Dynamics of entangled solutions of associating polymers. *Macromolecules* **2001**, *34* (4), 1058-1068.
- 24. Leibler, L.; Rubinstein, M.; Colby, R. H., Dynamics of reversible networks. *Macromolecules* **1991**, *24* (16), 4701-4707.
- 25. Stukalin, E. B.; Cai, L. H.; Kumar, N. A.; Leibler, L.; Rubinstein, M., Self-Healing of Unentangled Polymer Networks with Reversible Bonds. *Macromolecules* **2013**, *46* (18).
- 26. Rubinstein, M.; Semenov, A. N., Thermoreversible gelation in solutions of associating polymers. 2. Linear dynamics. *Macromolecules* **1998**, *31* (4), 1386-1397.
- 27. Indei, T.; Takimoto, J., Linear viscoelastic properties of transient networks formed by associating polymers with multiple stickers. *J Chem Phys* **2010**, *133* (19), 194902.
- 28. Chen, Q.; Zhang, Z.; Colby, R. H., Viscoelasticity of entangled random polystyrene ionomers. *Journal of Rheology* **2016**, *60* (6), 1031-1040.
- 29. Tang, S.; Wang, M.; Olsen, B. D., Anomalous self-diffusion and sticky Rouse dynamics in associative protein hydrogels. *J. Am. Chem. Soc.* **2015**, *137* (11), 3946-57.
- 30. Tang, S.; Habicht, A.; Li, S.; Seiffert, S.; Olsen, B. D., Self-Diffusion of Associating Star-Shaped Polymers. *Macromolecules* **2016**, *49* (15), 5599-5608.
- 31. Mahmad Rasid, I.; Holten-Andersen, N.; Olsen, B. D., Anomalous Diffusion in Associative Networks of High-Sticker-Density Polymers. *Macromolecules* **2021**, *54* (3), 1354-1365.
- 32. Ramirez, J.; Dursch, T. J.; Olsen, B. D., A Molecular Explanation for Anomalous Diffusion in Supramolecular Polymer Networks. *Macromolecules* **2018**, *51* (7), 2517-2525.
- 33. Rao, A.; Ramírez, J.; Olsen, B. D., Mechanisms of Self-Diffusion of Linear Associative Polymers Studied by Brownian Dynamics Simulation. *Macromolecules* **2021**, *54* (24), 11212-11227.
- 34. Fredlake, C. P.; Hert, D. G.; Kan, C. W.; Chiesl, T. N.; Root, B. E.; Forster, R. E.; Barron, A. E., Ultrafast DNA sequencing on a microchip by a hybrid separation mechanism that gives 600 bases in 6.5 minutes. *Proc Natl Acad Sci U S A* **2008**, *105* (2), 476-81.
- 35. Tang, S.; Olsen, B. D., Relaxation Processes in Supramolecular Metallogels Based on Histidine-Nickel Coordination Bonds. *Macromolecules* **2016**, *49* (23), 9163-9175.
- 36. Schmidt, B. V. K. J.; Hetzer, M.; Ritter, H.; Barner-Kowollik, C., Cyclodextrin-Complexed RAFT Agents for the Ambient Temperature Aqueous Living/Controlled Radical Polymerization of Acrylamido Monomers. *Macromolecules* **2011**, *44* (18), 7220-7232.
- 37. Boudara, V. A. H.; Read, D. J.; Ramírez, J., reptate rheology software: Toolkit for the analysis of theories and experiments. *Journal of Rheology* **2020**, *64* (3), 709-722.
- 38. Wang, M.; Timachova, K.; Olsen, B. D., Diffusion Mechanisms of Entangled Rod-Coil Diblock Copolymers. *Macromolecules* **2013**, *46* (14), 5694-5701.
- 39. Wang, M.; Timachova, K.; Olsen, B. D., Experimental Measurement of Coil-Rod-Coil Block Copolymer Tracer Diffusion through Entangled Coil Homopolymers. *Macromolecules* **2013**, *46* (4), 1651-1658.
- 40. Watanabe, H., Viscoelasticity and dynamics of entangled polymers. *Progress in Polymer Science* **1999**, *24* (9), 1253-1403.
- 41. Altukhov, Y. A.; Pokrovskii, V. N.; Pyshnograi, G. V., On the difference between weakly and strongly entangled linear polymers. *Journal of Non-Newtonian Fluid Mechanics* **2004**, *121* (2-3), 73-86.

- 42. Rubinstein, M.; Semenov, A. N., Dynamics of Entangled Solutions of Associating Polymers. *Macromolecules* **2001**, *34*, 1058-1068.
- 43. Carrillo, J.-M. Y.; Chen, W.-R.; Wang, Z.; Sumpter, B. G.; Wang, Y., Chain conformation of polymer melts with associating groups. *Journal of Physics Communications* **2019**, *3* (3), 035007.
- 44. Rao, A.; Yao, H.; Olsen, B. D., Bridging dynamic regimes of segmental relaxation and center-of-mass diffusion in associative protein hydrogels. *Physical Review Research* **2020**, *2* (4), 043369.
- 45. Jangizehi, A.; Ghaffarian, S. R.; Schmolke, W.; Seiffert, S., Dominance of Chain Entanglement over Transient Sticking on Chain Dynamics in Hydrogen-Bonded Supramolecular Polymer Networks in the Melt. *Macromolecules* **2018**, *51* (8), 2859-2871.
- 46. Zhang, X.; Liu, C.; Wang, Z., Force spectroscopy of polymers: Studying on intramolecular and intermolecular interactions in single molecular level. *Polymer* **2008**, *49* (16), 3353-3361.